JOURNAL OF GEOPHYSICAL RESEARCH, VOL. 111, B09316, doi:10.1029/2005JB004129, 2006

Does shear heating of pore fluid contribute to earthquake nucleation?

Paul Segall[1] and James R. Rice[2]

Received 29 October 2005; revised 5 April 2006; accepted 8 June 2006; published 29 September 2006.

[1] Earthquake nucleation requires reduction of frictional strength $\tau = \mu\,(\sigma - p)$ with slip or slip rate, where μ, σ_n, and p are the friction coefficient, normal stress, and fluid pressure, respectively. For rate state μ at fixed $(\sigma - p)$, instabilities can occur when $d\,\mu_{ss}/dv < 0$, where μ_{ss} is the steady state friction and v is slip rate. Shear heating increases p and, if dilatancy and pore pressure diffusion are limited, will cause τ to decrease. We examine how frictional weakening, shear heating, and dilatancy determine stability in simplified fault models. Mature faults have a thin (<1 mm) shear zone on which slip is concentrated, embedded within a ~0.1 m wide fault core with permeability of order 10^{-21} to 10^{-19} m^2, surrounded by rock of variable but higher permeability. Faults with $d\mu_{ss}/dv > 0$ are linearly stable at all wavelengths to adiabatic perturbations when v is near a plate rate if the wall rock permeability exceeds a critical value that is orders of magnitude less than inferred. Thus shear heating alone cannot then nucleate unstable slip; frictional weakening is required. However, shear heating can produce inertial instability on velocity strengthening faults following strong stress perturbations. On faults with $d\mu_{ss}/dv < 0$, shear heating increases pore pressure faster than is dissipated by Darcy flow at slip speeds of order 1 mm s^{-1}. For faults bounding half-spaces with uniform thermal and hydraulic properties, $\mu\,\dot{p}$ exceeds $\dot{\mu}\,(\sigma - p)$ during nucleation for slip speeds in excess of 10^{-2} to 10^{1} mm s^{-1}, depending on parameters chosen. Thus thermal effects are likely to dominate late in the nucleation process, well before seismic waves are radiated, as well as during fast seismic slip. By the time shear heating effects dominate, inertial slip is imminent (~10^{-1} s), so that time-to-failure calculations based on rate state friction are not biased by thermal pressurization.

Citation: Segall, P., and J. R. Rice (2006), Does shear heating of pore fluid contribute to earthquake nucleation?, *J. Geophys. Res.*, *111*, B09316, doi:10.1029/2005JB004129.

1. Introduction

[2] Earthquake nucleation and unstable fault slip require a reduction of frictional strength $\tau = \mu\,(\sigma - p)$ with slip or slip rate. Here τ is the shear resistance to slip, μ is the friction coefficient, σ is the fault normal stress and p is the pore fluid pressure within the fault zone. A substantial amount of complex physics underlies this seemingly simple relation. Extensive laboratory and theoretical work has been conducted to understand changes in μ with slip rate, slip, and slip history, giving rise to rate and state friction laws [*Dieterich*, 1979; *Ruina*, 1983]. At high slip rates, flash heating of microscopic asperity contacts may result in substantial decreases in friction coefficient [*Rice*, 1999, 2006; *Tullis and Goldsby*, 2003]. The normal stress σ may vary with slip if the fault is not planar, or with gradients in slip if the elastic properties vary across the fault [*Weertman*, 1980; *Andrews and Ben-Zion*, 1997], or if opening vibrations are trapped within the fault zone [*Brune et al.*, 1993]. Finally, pore fluid pressure may vary with slip due to a number of inelastic processes associated with shear in the fault zone, including dilatancy, pore compaction, and shear heating-induced thermal pressurization. Shear heating increases p and, if dilatancy and pore pressure diffusion are limited, will cause fault strength τ to decrease. During the propagation stage of the rupture, p may also vary with gradients in slip when permeability and poroelastic properties within the damage fringes vary across the fault [*Rudnicki and Koutsibelas*, 1991; *Rudnicki and Rice*, 2006], but this does not seem likely to affect nucleation and is not further considered here.

[3] The idea that shear heating will lead to thermal pressurization and a loss of frictional resistance was first proposed by *Sibson* [1973]. *Lachenbruch* [1980] analyzed the competing effects of dilatancy and pore pressure diffusion, which both act to mitigate against shear heating-induced increases in fault zone pore pressure. The subject was further explored by *Mase and Smith* [1987] and *Lee and Delaney* [1987] again in the context of imposed seismic

[1]Department of Geophysics, Stanford University, Stanford, California, USA.
[2]Department of Earth and Planetary Sciences and Division of Engineering and Applied Sciences, Harvard University, Cambridge, Massachusetts, USA.

0148-0227/06/2005JB004129$09.00

slip histories. *Sleep* [1995] considered the role of shear heating and frictional weakening in earthquake nucleation, but ignored fluid diffusion and dilatancy.

[4] The past several years have seen a resurgence of interest in shear heating. *Andrews* [2002] considered the effects of shear heating on dynamic rupture propagation. *Garagash and Rudnicki* [2003] analyzed a single degree of freedom system with slip weakening and shear heating-induced thermal pressurization. In their constitutive description, slip weakening and dilatancy ceases after a critical displacement, while thermally induced weakening continues with further slip. This leads to counterintuitive behavior in which (at least in some cases) enhanced weakening is stabilizing or enhanced dilatancy is destabilizing.

[5] *Rice* [1996] and *Lapusta and Rice* [2004] showed that shear heating may allow rupture propagation at low overall stress, on faults with local regions of low $\sigma - p$ where nucleation is easy, even though the fault strength is compatible with normal coefficients of friction and ambient hydrostatic pore pressure over the remainder of the fault. Stress concentrations at the rupture front are sufficient to initiate slip, yet the average stress doing work against fault slip is low, consistent with the absence of a thermal anomaly along the San Andreas Fault.

[6] *Rice* [2006] has recently shown that the earthquake fracture energies estimated from seismic observables are plausibly consistent with theoretical expectations for shear heating-induced thermal pressurization. While the seismological estimates of fracture energy are not without assumptions, they are independent of the theoretical predictions. This result strongly suggests that thermal pressurization be seriously considered as a weakening mechanism during dynamic rupture.

[7] There remains, however, a great deal of uncertainty about the important weakening mechanisms in earthquakes, or which mechanisms dominate under given conditions. For example, whether frictional weakening dominates at low slip speeds, and thermal pressurization at high slip speeds, or whether different processes dominate in different geologic settings. There is a sense in the community that thermal pressurization effects are significant only for moderate to large earthquakes. *Kanamori and Heaton* [2000, p. 147] stated that "A modest ΔT of 100–200°C would likely increase the pore pressure enough to significantly reduce friction for earthquakes with $M_w = 3$ to 4." *Andrews* [2002] defines a threshold propagation distance, dependent on permeability, at which thermal pressurization effects dominate over frictional weakening. For hydraulic diffusivities of 0.02 $m^2\ s^{-1}$ (greater by $\sim 10^4$ than that inferred from data taken from ultracataclastic rocks, discussed below) and other parameters chosen, he estimates the transition from slip weakening to shear heating dominated weakening occurs after roughly 300 m of propagation, corresponding to M_w 3.5. For the lower diffusivities inferred from lab data on ultracataclasites, the threshold magnitude range and propagation distance would be significantly lower.

[8] The previously mentioned studies highlight the importance of the permeability of the fault zone and its surroundings in controlling thermally induced pore pressure changes. If the permeability is sufficiently high, pore fluid diffuses out of the fault zone preventing pore pressures from increasing substantially. Recent studies have measured the permeability of fault zone materials at effective stresses representative of seismogenic depths. *Wibberley and Shimamoto* [2003] measured the permeability of fault zone materials from the Median Tectonic Line in Japan. They identify a central shear zone on the order of a few millimeters in thickness in which most of the deformation is believed to be concentrated. Surrounding this is a ultracataclastic fault core roughly 0.1 m in thickness, which is in turn bordered by foliated gouges, cataclasites, and fractured mylonites. Permeability of the fault core was found to be in the range 10^{-21} to 10^{-19} m^2 at effective confining stresses of 80 to 180 MPa. The permeability is quite variable in the surrounding rocks, reaching as high as 10^{-15} to 10^{-16} m^2 but locally as low as 10^{-19} to 10^{-18} m^2. *Lockner et al.* [2000] measured the permeability of drill core samples from the Nojima fault, source of the Kobe earthquake, at depths of up to 1500 m. Permeabilities as determined in the laboratory at an effective isotropic confining pressure of 50 MPa are 10^{-19} to 10^{-18} m^2 within the narrow fault core, whereas the surrounding damage zone, tens of meters in width, has permeabilities of 10^{-17} to 10^{-16} m^2.

[9] The viewpoint that slip on a mature fault is principally hosted within a narrow zone, less than a few millimeters in thickness, itself within an ultracataclastic zone of tens of millimeters to perhaps 100 mm thickness that is bordered by a less finely granulated damage zone, is also supported by studies of the North Branch San Gabriel fault [*Chester et al.*, 1993] and Punchbowl fault [*Chester and Chester*, 1998] of the San Andreas system. By mature we mean a fault that has accommodated significant offset, has localized to a quasi-steady state structure, and is capable of producing large earthquakes. *Sibson* [2003] also summarizes observations for localized shear within fault zones.

[10] Note that the permeability distributions inferred here are entirely consistent with field observations of highly conductive fault zones, as summarized, for example, by *Townend and Zoback* [2000]. As noted by *Lockner et al.* [2000] the damage zone acts as a high-permeability conduit for flow parallel to the fault, whereas the low-permeability fault core will impede fluid flow perpendicular to the fault.

[11] Following our earlier analysis [*Segall and Rice*, 1995], we explore the interaction of rate and state variable friction, with shear heating, dilatancy, and hydraulic diffusion, with the inclusion of shear heating being the new ingredient here. The specific questions we address are the following: (1) Can shear heating-induced pore pressurization nucleate unstable slip on a fault that exhibits either no frictional weakening, or steady state velocity strengthening? (2) If the fault is steady state velocity weakening, does the frictional instability or the shear heating instability dominate? (3) If frictional weakening nucleates the instability at what point (displacement, slip speed) does thermal weakening nevertheless become the dominant weakening mechanism?

2. Constitutive Equations

[12] Following *Segall and Rice* [1995], we let $m = \rho\phi$ be the mass of pore fluid per unit volume that the fault zone material occupied in its initial or reference state, and write its rate as $\dot{m} = \rho\,\dot{\phi} + \phi\,\dot{\rho}$. Here ρ is fluid density within the

pore space and ϕ is "porosity" which, more precisely in our context, is the ratio of the current pore volume to the overall volume that the porous medium occupied in the reference state. The fluid density is a function of both pressure and temperature, and so its rate is

$$\dot{\rho} = \rho\beta_f\dot{p} - \rho\lambda_f\dot{T}, \tag{1}$$

where the fluid compressibility and thermal expansivity are defined as

$$\beta_f = \frac{1}{\rho}\left(\frac{\partial\rho}{\partial p}\right)_T \qquad \lambda_f = -\frac{1}{\rho}\left(\frac{\partial\rho}{\partial T}\right)_p. \tag{2}$$

Both the compressibility and expansivity are functions of pressure and temperature [e.g., *Lachenbruch*, 1980, *Garagash and Rudnicki*, 2003]. Following these authors, and assuming hydrostatic pore pressures, and geothermal gradients of 20 to 25°C km^{-1}, we estimate $\beta_f \approx 6 \times 10^{-10}$ Pa^{-1} and $\lambda_f \approx 1 \times 10^{-3}$ °C^{-1}. (Symbol definitions and representative values are listed in the notation section.)

[13] We consider conditions of constant fault-normal stress σ and vanishing fault-parallel straining. The porosity can then be separated into an inelastic part, ϕ_{plastic} [*Segall and Rice*, 1995], which would be the porosity remaining if pore pressure and temperature were returned, elastically and reversibly, to their initial values, and a thermoelastic part due to the changes in pressure and temperature from those initial values. Thus the rate of change is

$$\dot{\phi} = \phi\beta_\phi\dot{p} + \phi\lambda_\phi\dot{T} + \dot{\phi}_{\text{plastic}}, \tag{3}$$

where the pressure expansivity and thermal expansivity of the pore space are defined by

$$\beta_\phi = \frac{1}{\phi}\left(\frac{\partial\phi}{\partial p}\right)_T \qquad \lambda_\phi = \frac{1}{\phi}\left(\frac{\partial\phi}{\partial T}\right)_p. \tag{4}$$

Pore pressure expansivity is a function of pore shape; estimates are given by *Segall and Rice* [1995] and *Wibberley* [2002] on the order of 1×10^{-9} Pa^{-1}. For elastic response of fault wall gouge, *Rice* [2006] estimates a value of $\sim 0.6 \times 10^{-9}$ Pa^{-1} for an effective confining pressure of 126 MPa, assuming the fault normal stress is constant and that there is no strain parallel to the fault. Following the same procedure he estimates a thermal expansivity of the pore space that is opposite in sign and a factor of 5 to 8 larger than the thermal expansivity of the solid phase (typically of the order of 2×10^{-5} °C^{-1} [e.g., *Mase and Smith*, 1987]). The sign difference results because the thermal expansion of the pore space is more than compensated by the large fault parallel compression induced by the thermal expansion with the boundary condition of vanishing fault parallel strain. *Rice* [2006] estimates λ_ϕ of -2×10^{-4} °C^{-1}, still an order of magnitude less, in magnitude, than the pore fluid expansivity. Combining the above leads to a fluid mass rate of change given by

$$\dot{m} = \rho_0\phi_0\left[\left(\beta_f + \beta_\phi\right)\dot{p} - \left(\lambda_f - \lambda_\phi\right)\dot{T}\right] + \rho_0\dot{\phi}_{\text{plastic}}, \tag{5}$$

where the subscript zeros denote properties in the reference state and the β and λ are treated as constants.

[14] Extensive laboratory measurements show that for constant p and σ the frictional resistance to sliding depends on the instantaneous slip speed v, and the state of the slip surface as characterized by one or more state variables θ. A widely used form for the constitutive relation is [*Ruina*, 1983; *Kilgore et al.*, 1993]

$$\tau = (\sigma - p)\left[\mu_0 + a\ln\frac{v}{v^*} + b\ln\frac{\theta v^*}{d_c}\right], \tag{6}$$

where a and b are material constants, v^* is an arbitrary normalizing constant, and μ_0 is the nominal friction ($\mu = \mu_0$ for $v = v^*$ and $\theta = d_c/v^*$).

[15] In this study we use the "aging," or "slowness," form of the state evolution equation [*Ruina*, 1983] given by

$$\frac{d\theta}{dt} = 1 - \frac{\theta v}{d_c}, \tag{7}$$

where d_c is the characteristic displacement over which the state variable (interpreted to be average asperity contact lifetime) evolves. θ evolves exponentially toward steady state with a characteristic time of d_c/v. (An alternate "slip" form of the state evolution equations $\dot{\theta} = -(\theta v/d_c)\ln(\theta v/d_c)$ has also been widely studied [*Rice and Ruina*, 1983; *Rice and Gu*, 1983; *Marone*, 1998].) In either case, the steady state frictional resistance is given by

$$\tau_{ss} = (\sigma - p)\left[\mu_0 + (a - b)\ln\left(\frac{v_{ss}}{v^*}\right)\right]. \tag{8}$$

Following *Segall and Rice* [1995], we assume a constitutive equation for the inelastic part of the porosity, motivated in part by experiments of *Marone et al.* [1990], linking it uniquely to the average lifetime of current contacts by

$$\phi_{\text{plastic}} = \phi_0 - \varepsilon\ln\left(\frac{v^*\theta}{d_c}\right), \tag{9}$$

where ε is of the order of 10^{-4} for the *Marone et al.* [1990] gouge. From (9) and (7), ϕ_{plastic} decreases with the logarithm of time when $v = 0$, but approaches a constant value in sustained slip at a constant rate v, $(\phi_{\text{plastic}})_{ss} = \phi_0 + \varepsilon\ln(v/v^*)$.

3. Thermal Transport Equations

[16] We consider the model fault system shown in Figure 1 in which the shearing deformation is localized in a narrow zone of thickness h. The shear zone is located in $-h < y < 0$, and we assume that there are no variations in thermal properties parallel to the fault (x direction). The general energy equations are

$$\tau\dot{\gamma} - \frac{\partial q_h}{\partial y} = \rho_{\text{total}}c_v\frac{\partial T}{\partial t}, \tag{10}$$

where $\dot{\gamma}$ is the shear strain rate, q_h is the heat flux in the y direction (heat flow in the x direction is assumed

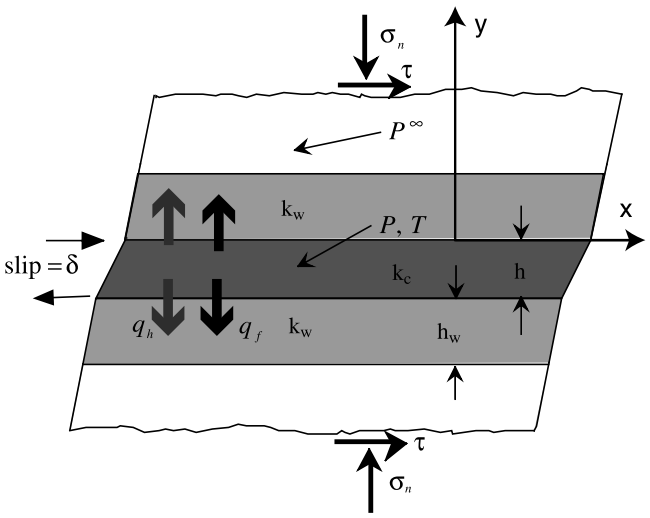

Figure 1. Simplified fault zone model, model I. Narrow principal shear zone of thickness h is embedded in a low-permeability fault core with half thickness h_w. The permeability of the wall rocks is k_w, whereas k_c denotes the permeability of the fault core. The surrounding rocks are of variable but generally greater permeability; q_h and q_f represent the heat flux and fluid mass flux out of the central shear zone. The pore pressure outside the fault core is assumed to be kept constant at p^∞ by the large permeability and small amounts of fluid transported out of the fault core. For fault model II the central shear zone thickness $h \to 0$, and the permeability is uniform.

negligible), ρ_{total} is the total density (solid plus pore fluid), and c_v is the heat capacity per unit mass. Fourier's law states

$$q_h = -\mathcal{K}\frac{\partial T}{\partial y}, \tag{11}$$

where $\mathcal{K}$ is the thermal conductivity. Outside of the shear zone where heat production can be neglected, (10) and (11) together yield a diffusion equation

$$\frac{\partial T}{\partial t} - c_{th}\frac{\partial^2 T}{\partial y^2} = 0 \qquad y > 0, y < -h, \tag{12}$$

where $c_{th} = \mathcal{K}/\rho_{\text{total}}c_v$ is the thermal diffusivity. Energy balance for the fault zone requires that the heat generated by fault slip ($\dot{\gamma} = v/h$) either accumulate within the fault zone or be transported into the surrounding rock mass. Thus the thickness averaged energy balance, again ignoring heat flow parallel to the fault, is

$$2q_h(y=0) + \rho_{\text{total}}c_v h\frac{\partial T}{\partial t} = \tau v \qquad -h < y < 0, \tag{13}$$

where $q_h(y = 0)$ is the net flux of heat out of the fault zone, the factor of 2 accounts for the other boundary at $y = -h$, and T is understood to be the average temperature in the shear zone. The boundary conditions on (12) and (13) are that the temperature and heat fluxes match at $y = 0$. Combining (11) with (13) yields

$$-2\mathcal{K}\left.\frac{\partial T}{\partial y}\right|_{y=0} + \rho_{\text{total}}c_v h\frac{\partial T}{\partial t} = \tau v \qquad -h < y < 0. \tag{14}$$

For short times $t \ll h^2/4c_{th}$ the shear zone is adiabatic and for constant shear stress and slip speed the temperature, from (14), increases linearly in time. For times $t \gg h^2/4c_{th}$ the effect of the finite shear zone thickness can be neglected and for constant shear stress and slip speed the solution to (12) and (14), for temperature rise, increases as

$$T(y=0) = \frac{\tau_0 v_0}{\rho_{\text{total}}c_v}\sqrt{\frac{t}{\pi c_{th}}}. \tag{15}$$

[17] *Lachenbruch* [1980] gives a value of 0.24 cal g^{-1} °C for the heat capacity, which yields $\rho_{\text{total}}c_v \sim 2.7$ MPa °C^{-1}. For a typical rock conductivity of 2.4 W m°C^{-1} [e.g., *Sleep and Fujita*, 1997] this yields a thermal diffusivity of $\sim 10^{-6}$ m^2 s^{-1}. For shear zone thicknesses h of 3 mm or less, the critical time $h^2/4c_{th}$ is 2 s, or less. Thus, for times greater than a few tens of seconds we can safely neglect the effect of the narrow shear zone on the temperature distribution. In this limit, equivalent to $h \to 0$, equation (14) becomes a boundary condition on the heat equation (12).

4. Fluid Transport Equations

[18] We further consider the model fault system shown in Figure 1 which, based on the field and laboratory studies, consists of a thin shear zone, thickness h, bordered by a low-permeability wall zone (which comprises the remainder of the ultracataclasite fault core) of thickness h_w. Outside the low-permeability wall zone there is a much more permeable damage zone. Conservation of pore fluid mass requires

$$\nabla \cdot q_f + \frac{\partial m}{\partial t} = 0, \tag{16}$$

where q_f is the fluid mass flux. Considering only flux perpendicular to the fault zone, Darcy's law is

$$q_f = -\frac{\rho\kappa}{\nu}\frac{\partial p}{\partial y}, \tag{17}$$

where κ is the permeability and ν is the fluid viscosity. Combining (16) and (17) with (5) yields a diffusion equation

$$c_{\text{hyd}}\frac{\partial^2 p}{\partial y^2} - \frac{\partial p}{\partial t} = -\Lambda\frac{\partial T}{\partial t} + \frac{\dot{\phi}_{\text{plastic}}}{\beta}. \tag{18}$$

Here c_{hyd} is the hydraulic diffusivity, $c_{\text{hyd}} = \kappa/\beta\nu$, β is the effective compressibility, and Λ is the ratio of expansivity to compressibility,

$$\begin{aligned}\beta &= \phi(\beta_f + \beta_\phi)\\ \Lambda &= \left(\frac{\lambda_f - \lambda_\phi}{\beta_f + \beta_\phi}\right).\end{aligned} \tag{19}$$

For a porosity of 0.05, β is in the range 5 to 8 $\times$ 10^{-11} Pa^{-1}, whereas representative values for Λ are 0.6 to 1.1 MPa $°C^{-1}$ [*Rice*, 2006].

[19] Fluid mass conservation within the shear zone, of thickness h, requires

$$2q_f(y=0) + h\frac{\partial m}{\partial t} = 0, \tag{20}$$

where $q_f(y = 0)$ is the net flux of pore fluid out of the shear zone, and $\dot{m}$ is the fluid mass accumulation rate per unit thickness of fault core. Combining (20) and (17) with (5) yields

$$\frac{\partial p}{\partial t} = \Lambda\frac{\partial T}{\partial t} - \frac{\dot{\phi}_{\text{plastic}}}{\beta} - \frac{2c_w}{h}\left.\frac{\partial p}{\partial y}\right|_{y=0}, \tag{21}$$

where c_w is the hydraulic diffusivity of the low-permeability wall rocks bordering the shear zone. At the boundary between the narrow shear zone and the remainder of the low-permeability fault core (and all other similar boundaries) the pore pressures and fluid mass fluxes must be continuous.

[20] It is worth noting some characteristic times for the problem under consideration. The first is the characteristic time for pore fluid flow out of the narrow shear zone of thickness h, $t = h^2/4c_w$, where c_w is the hydraulic diffusivity of the narrow low permeability band bordering the shear zone. On the basis of references cited in section 1 we chose fault core permeabilities on the order of 10^{-20} to 10^{-19} m^2. The viscosity of water at the relevant temperatures and pressures is roughly 10^{-4} Pa s. Thus the hydraulic diffusivity of the fault core is of the order $\kappa/\nu\beta \sim 10^{-5}$ -10^{-6} m^2 s^{-1}. For h less than or equal to 3 mm, the characteristic diffusion time is 0.2 to 2 s.

[21] The relatively high permeability outside the fault core (order of 10^{-15} to 10^{-16} m^2) suggests that this zone remains at nearly constant pore pressure, p^∞. At times long compared to the characteristic diffusion time across the low permeability fault core we can approximate $\partial p/\partial y|_{y=0}$ in (21) with $(p - p^\infty)/h_w$, [e.g., *Segall and Rice*, 1995; *Garagash and Rudnicki*, 2003] where p is the pore pressure in the shear zone, so that (21) becomes

$$\dot{p} = \Lambda\dot{T} - \frac{\dot{\phi}_{\text{plastic}}}{\beta} - \frac{2c_w}{hh_w}(p - p^\infty). \tag{22}$$

The terms on the right-hand side of (22) represent thermal pressurization, dilatancy, and pore fluid diffusion, respectively. Note that the combination of constants in front of the pressure difference term is interpreted as the inverse of a characteristic diffusion time, i.e.,

$$\frac{2c_w}{hh_w} \equiv c^* = \frac{1}{t_f} = \frac{\kappa}{\nu\beta}\frac{2}{hh_w}. \tag{23}$$

For numbers cited above and $h_w \sim 0.1$ m, the characteristic timescale for fluid diffusion is on the order of 10^1 to 10^2 s. The diffusion timescales can be compared to the time scale for the earthquake nucleation process. From the results of *Dieterich* [1992], discussed below, nucleation times scale with d_c/v_0, where v_0 is the initial velocity. Assuming nucleation starts when the slip speed equals the plate rate, and using laboratory values of d_c, the nucleation times are of the order of 10^4 to 10^5 s, considerably longer than the diffusion time across the low-permeability, ultracataclasite fault core, suggesting that (22) is a reasonable approximation.

[22] On the other hand, slip speed increases extremely rapidly as inertial instability is approached. For example the characteristic time for the fault to reach instability from speeds of 10 μm s^{-1} is, from d_c/v_0, only 1 to 10 s. At times less than t_f, given by (23) the pore pressure senses only the low-permeability fault core, and can thus be approximated by diffusion into a half-space with the diffusivity of the fault core. In this limit, with $h \to 0$, the governing equation is (18), with dilatancy of the wall rocks typically ignored. In the limit $h \to 0$ equation (21) becomes a boundary condition on (18), $\partial p/\partial y|_{y=0} = 0$.

[23] In the remainder of the paper, we will find it useful to make use of two transport models for which solutions are relatively tractable. In model I the thermal regime is adiabatic, and we account explicitly for the low-permeability fault core as in (22). The fault zone pore pressure thus follows

$$\frac{\partial p}{\partial t} = \frac{\Lambda\tau v}{\rho_{\text{total}}c_v h} - \frac{\dot{\phi}_{\text{plastic}}}{\beta} - \frac{2c_w}{hh_w}(p - p^\infty). \tag{24}$$

Model II treats the thermal and hydraulic properties as homogeneous and takes the limit of zero fault zone thickness. In this case it can be shown [*Rice*, 2006] that temperature and pressure are uniquely related through

$$p(y=0,t) = \frac{\Lambda T(y=0,t)}{1 + \sqrt{c_h/c_{th}}}. \tag{25}$$

It can also be shown that the temperature change on fault due to shear heating is given by [e.g., *Carslaw and Jaeger*, 1959]

$$T(y=0,t) = \frac{1}{\sqrt{2\pi}}\frac{1}{\rho c}\int_0^t \frac{\tau(t')v(t')dt'}{\sqrt{2c_{th}(t-t')}}. \tag{26}$$

5. Elastic Loading System

[24] For a two-dimensional fault with spatially uniform slip that is loaded by a uniform far-field velocity v^∞ some distance L from the fault, the shear stress acting on the fault is given by $\tau = G(v^\infty t - u)/(2L)$ where G is shear stiffness. This is the same representation as a single degree of freedom, spring slider model

$$\tau = k(v^\infty t - u), \tag{27}$$

where $k = G/(2L)$ is the spring stiffness, v^∞ is the load point velocity, and u is the slider displacement. In three

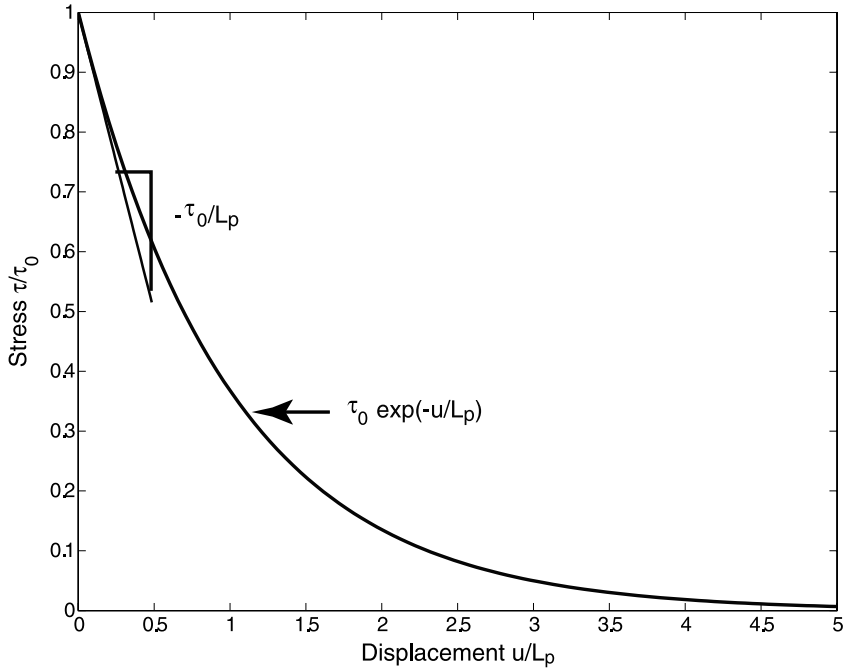

Figure 2. Decay of fault zone strength with fault slip for undrained adiabatic conditions with constant frictional properties and no dilation. The slope of the curve evaluated at $u = 0$ gives the critical spring stiffness.

dimensions with slip on a circular fault patch of radius r the appropriate spring stiffness is

$$k = \frac{7\pi G}{24r}. \tag{28}$$

More generally the shear stress on the fault subject to quasi-static loading can be represented by $\tau = \tau^{\infty} + \tau^{\text{int}}$, where τ^{∞} is the loading stress and τ^{int} represents elastic stress interactions due to nonuniform slip. For a two-dimensional fault loaded uniformly at distance L from the fault, $\tau^{\infty} = G(v^{\infty}t - \bar{u})/(2L)$ where $\bar{u}$ is the spatially uniform part of the slip. For antiplane deformation in a homogeneous elastic half-space the stress interactions due to nonuniform slip s are given by a Hilbert transform of the slip gradients

$$\tau^{\text{int}} = \frac{G}{2\pi}\int_{-\infty}^{\infty}\frac{-\partial s/\partial\xi}{x-\xi}d\xi. \tag{29}$$

For plane strain deformation G is replaced by $G/[2(1 - \nu_P)]$, where ν_P is Poisson ratio.

[25] Fourier transforming in the along-strike dimension, the interaction stress becomes $\hat{\tau}\ (m) = -\hat{k}(m)\ \hat{u}$, where $\hat{}$ indicates transformed variables and $\hat{k}(m)$ is an effective stiffness dependent on wave number m. For a uniform half-space, as in (29), $k = G|m|/2$. More generally for an isotropic elastic material subjected to antiplane loading with constant velocity condition imposed at distance L from the fault $k(m) = G|m|/[2\tanh(|m|L)]$ [*Rice and Ruina*, 1983].

[26] In summary, there are significant cases of interest in which the elasticity relations at each Fourier mode are the same form as (27). First, if we consider perturbations of slip, stress, and pore pressure from steady state values, the uniform steady velocity cancels the loading term and the stress at each Fourier mode is $\hat{\tau}\ (m) = -\hat{k}(m)\hat{u}$. Second, when considering earthquake nucleation the timescale is such that remote loading may be neglected and the stress can be expressed as $\hat{\tau}\ (m) = \tau^{\infty} - \hat{k}(m)\hat{u}$, with τ^{∞} constant.

6. Undrained Adiabatic Slip With Constant Friction and No Dilatancy

[27] In the limit of no fluid transport (undrained) and no heat transport (adiabatic), equations (22) and (14) reduce to

$$\frac{dp}{dt} = \frac{\mu_0\Lambda(\sigma - p)}{\rho_{\text{total}}c_v h}\frac{du}{dt}, \tag{30}$$

where μ_0 is the constant friction coefficient. Noting that for fixed normal stress, $\dot{\tau} = -\mu_0\dot{p}$, (30) can be written as $\dot{\tau} = -(\tau/L_p)\ \dot{u}$, which integrates directly to

$$\tau(u) = \tau_0 e^{-u/L_p}, \tag{31}$$

where L_p is the characteristic slip weakening distance for weakening due to thermal pressurization,

$$L_p = \frac{\rho_{\text{total}}c_v h}{\mu_0\Lambda}, \tag{32}$$

demonstrating that under these circumstances, shear heating causes the strength to decay exponentially with slip (Figure 2), as earlier noted by *Lachenbruch* [1980].

[28] Given our earlier estimates of $\Lambda \sim 0.7$ MPa $^{\circ}\text{C}^{-1}$ and $\rho_{\text{total}}\ c_v \sim 2.7$ MPa $^{\circ}\text{C}^{-1}$, equation (32) leads to L_p being roughly 6 times the thickness of the slip zone. If we take that to be on the order of 2–3 mm, then L_p is on the order of 12–18 mm.

[29] The temperature evolution is then given by

$$\frac{dT}{du} = \frac{\tau}{\mu_0 \Lambda L_p} = \frac{(\sigma - p_0)}{\Lambda L_p} e^{-u/L_p}, \tag{33}$$

which can be integrated to give

$$T - T_0 = \frac{(\sigma - p_0)}{\Lambda}\left(1 - e^{-u/L_p}\right). \tag{34}$$

The maximum temperature rise is thus $(\sigma - p_0)/\Lambda$ and for the values we have given yields a few hundred degrees Celsius. This is generally insufficient to cause melting, unless rapid fluid drainage occurs and the frictional resistance remains high during slip.

[30] Given the displacement-dependent strength decay in (31) stress equilibrium on the fault requires

$$\tau_0 - ku - \tau_0 e^{-u/L_p} = \eta \frac{du}{dt}, \tag{35}$$

where τ_0 is the initial stress, k is stiffness, and $\eta = G/2v_s$ is a radiation damping coefficient, where v_s is the s wave velocity. Equation (35), when linearized about $u = 0$, has stable response to small perturbation from $u = \dot{u} = 0$ when $k > \tau_o/L_p$, and unstable response when $k < \tau_o/L_p$. Treated nonlinearly, it has no solution with $\dot{u} \geq 0$ (required, because backslip is disallowed) when $k > \tau_o/L_p$. Thus τ_o/L_p is the critical stiffness. Note that we must imagine that the initial stress slightly exceeds the strength in order to exclude the static $u = du/dt = 0$ solution.

[31] While the focus of this paper is on earthquake nucleation, it is interesting to consider the behavior of (35) after rapid slip is well underway. It is straightforward to show that the slip and slip rate at maximum velocity are

$$u_{\text{maxvel}} = L_p \ln\left(\frac{\tau_0}{kL_p}\right)$$
$$v_{\max} = \frac{1}{\eta}\left\{\tau_0 - kL_p\left[1 + \ln\left(\frac{\tau_0}{kL_p}\right)\right]\right\}. \tag{36}$$

The ratio of slip u_{maxvel} to velocity $v_{\max}$ gives an estimate of the time to peak velocity. At nucleation the stiffness is likely to be close to the critical value for nucleation. However, as the slipping zone expands, k decreases, such that $k\,L_p/\tau_0 \ll 1$. In this limit the time to maximum velocity is

$$t_{\text{maxvel}} \approx \frac{u_{\text{maxvel}}}{v_{\max}} \approx \frac{GL_p}{2v_s\tau_0} \ln\left(\frac{\tau_0}{L_p k}\right). \tag{37}$$

For displacements $u/L_p \gg 1$ the fault strength decays to zero and the exponential term in (35) can be ignored. This leads to

$$u = \frac{\tau_0}{k}\left[1 - \exp\left(\frac{-kt}{\eta}\right)\right]. \tag{38}$$

This approximation and the approximation for the time to peak velocity (37) become increasingly accurate for small kL_p/τ_0/(Figure 3). (Of course, the solution (38) simply reflects the balance between elastic unloading and the radiation damping approximation to elastodynamics and thus applies to any situation in which the fault strength vanishes with increasing slip.) The maximum displacement $\tau_0/k = 2\tau_0\ l/G$, where l is the half length of the fault. The risetime is $\eta/k = l/v_s$, the time it takes for s waves to traverse the fault. For l = 1km the risetime is 0.3 s. The time to peak velocity is very short; for $G = 3 \times 10^4$ MPa, $v_s = 3$ km s^{-1}, $L_p = 0.01$ m, and $\tau_0 = 60$ MPa, the time to peak velocity is on the order of tens of milliseconds, indicating a very rapid acceleration under undrained adiabatic conditions.

7. Can Nucleation Occur by Shear Heating Alone?

[32] We now address the question of whether shear heating can nucleate an instability on a velocity strengthening fault. To do so, we conduct a linearized stability analysis following the procedure outlined for the isothermal case by *Segall and Rice* [1995]. At quasi-static equilibrium the frictional resistance and elastic driving stress are balanced

$$(\sigma - p^\infty)\mu(v, \theta) = k(v^\infty t - u). \tag{39}$$

At steady state the constant stress condition requires $v = v^\infty$. The steady state values of pore pressure, porosity, and state are given by $p_{ss} = p^\infty$, $\phi_{ss} = \phi_0 + \varepsilon \ln(v^\infty/v^*)$, and $\theta_{ss} = d_c/v^\infty$. At steady state, heat conduction exactly balances the rate of frictional work, $2q_h = \tau_{ss}\, v_{ss}$, such that $\dot{T} = 0$ in (13). In this section we consider the limiting case of adiabatic perturbations. This is conservative in the sense that if the fault system is stable to adiabatic perturbations, then it is certainly stable if that assumption is relaxed and heat is allowed to conduct away from the fault. Decreasing the temperature in the fault zone diminishes the amount of thermal pressurization and is therefore stabilizing.

[33] For adiabatic perturbations the energy equation becomes

$$\tau v - \tau_{ss} v_{ss} = \rho_{\text{total}} c_v h \frac{\partial T}{\partial t}, \tag{40}$$

where the unsubscripted variables refer to instantaneous values, whereas τ_{ss} and v_{ss} refer to steady state values. The details of the perturbation analysis are given in Appendix A.

[34] As a first step consider the case of undrained adiabatic deformation with constant coefficient of friction. As remarked in section 6, and shown in Appendix A, instabilities can only occur when the system stiffness is less than a critical value given by

$$k_{\text{uacf}} = \mu_0(\sigma - p)/L_p, \tag{41}$$

where the notation k_{uacf} refers to undrained adiabatic (and no dilatancy) with constant friction. This result is sensible in that it gives the slope of the displacement weakening curve given by (31) at zero displacement (Figure 2). If the stiffness is less than the critical value, the stresses are unbalanced in a direction of positive displacement following a small increment of slip.

[35] The critical stiffness including the effects of dilatancy is shown in Appendix A to be $\mu_0(\sigma - p)/(L_p + d_c)$.

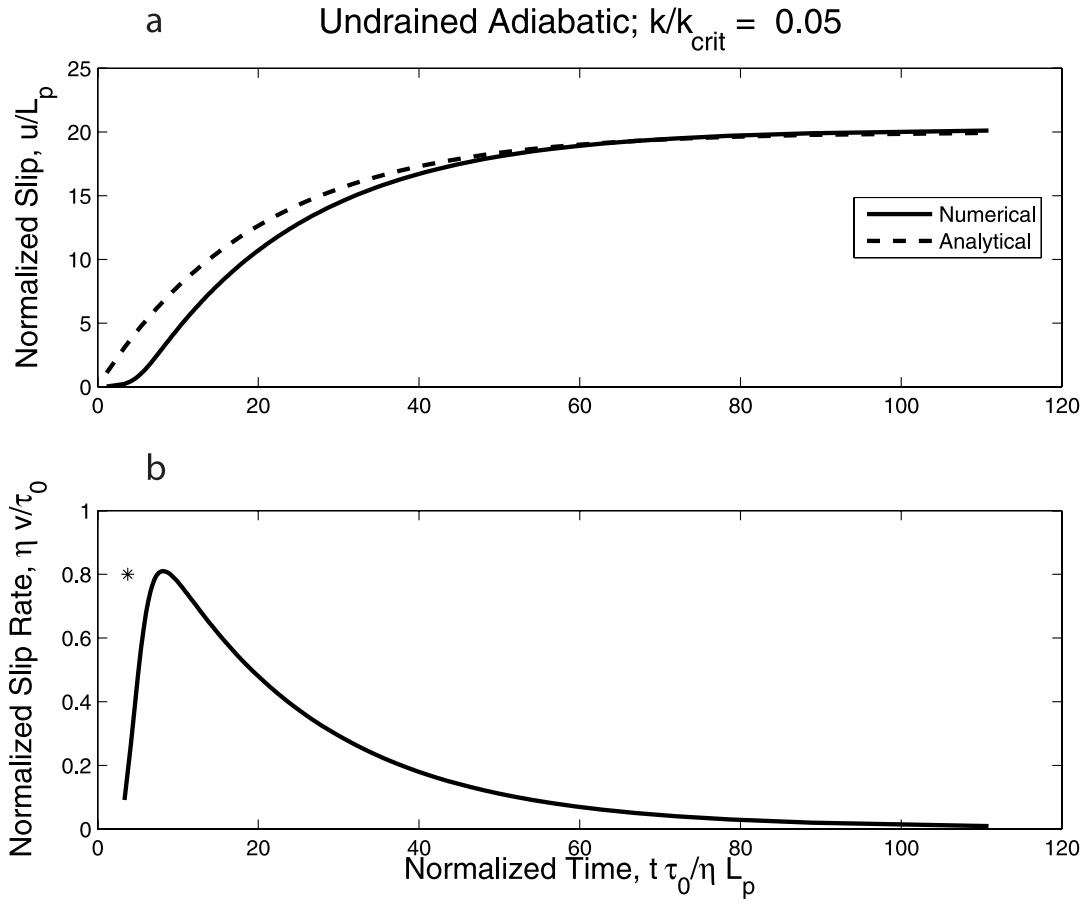

Figure 3. Slip history for undrained adiabatic conditions with constant friction. (a) Normalized displacement as a function of normalized time. The numerically integrated equations are compared to the approximation given by (38). (b) Normalized slip velocity as a function of normalized time. The peak velocity and time of peak velocity, given by equations (36) and (37), are shown by the asterisk.

Curiously, the dilatancy coefficient ϵ does not enter. It does, however, influence the frequency of oscillations at neutral stability.

[36] The critical stiffness above (41) can be compared to that for drained isothermal conditions (or drained adiabatic, there is no difference) given by *Ruina* [1983] for steady state velocity weakening conditions ($(b - a) > 0$):

$$k_{di} = (b - a)(\sigma - p)/d_c, \tag{42}$$

where the subscript *di* stands for drained isothermal so that the ratio k_{di}/k_{uacf} is $(b - a)L_p/\mu_0\, d_c$. Taking $b - a \sim 2 \times 10^{-3}$, $\mu_0 \sim 0.6$, $L_p \sim 10$ mm, and $d_c \sim 0.02$ mm suggests a ratio of order unity. This alone suggests that shear heating could play an important role in earthquake nucleation; however, in order to properly answer this question we need to consider the effects of fluid diffusion, which decreases the fault zone pore pressure and diminishes the thermal weakening effect.

[37] We generalize the previous results by adding pore pressure diffusion and the direct effect in the friction law $a > 0$, but retain the assumptions of no state evolution effect, $b = 0$, and no dilatancy $\epsilon = 0$. Note that relaxing these restrictions will cause the system to become even more stable. That is, $b > 0$ decreases the steady state velocity strengthening (for assumed $a > b$), and dilatancy ($\epsilon > 0$) tends to decrease the pore pressure and is thus stabilizing. Thus, if the system is linearly stable under these conditions it is certainly stable when they are relaxed.

[38] In Appendix A we show that the critical stiffness in this case reduces to

$$k_{sa} = \frac{\tau_0}{L_p} - \frac{a(\sigma - p)c^*}{v_0}. \tag{43}$$

Thus, for adiabatic, velocity strengthening faults ($b = 0$) without dilatancy, the critical stiffness decreases linearly with hydraulic diffusivity. In particular, the critical stiffness vanishes for $c^* = \mu_0 v_0/aL_p$. For diffusivities greater than this, slip is stable regardless of the elastic stiffness of the system.

[39] We can generalize this result further by allowing for $b > 0$ (but still velocity strengthening, in that $a > b > 0$) and dilatancy. Following the arguments in Appendix A, we find that the critical diffusivity that causes the critical stiffness to vanish is given by

$$c^*_{\text{crit}} = \frac{\mu_0 v_0}{(a - b)L_p}, \tag{44}$$

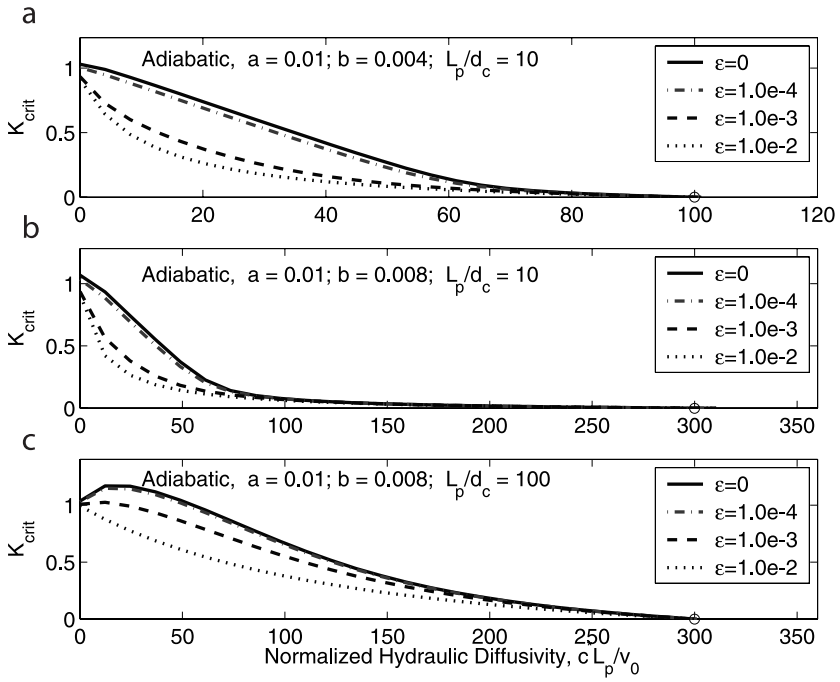

Figure 4. Critical spring stiffness as a function of hydraulic diffusion time for adiabatic deformation of a steady state velocity strengthening fault. Critical stiffness is normalized by the critical stiffness for undrained, adiabatic slip with constant friction and no dilatancy $\mu_0(\sigma - p)/L_p$. Systems with stiffness less than the critical value (below the appropriate curve) are linearly unstable.

which is only modestly different from the result obtained when ignoring weakening effects and dilatancy (replace a by $a - b$ in the critical value obtained by (43)). Again, the critical diffusivity does not depend on the dilatancy coefficient.

[40] Taking $\mu_0 \approx 0.6$, $L_p \sim 0.01$ m, $a - b \approx 4 \times 10^{-3}$, and $v_0 \sim 30$ mm yr^{-1} $\approx 10^{-9}$ m s^{-1}, and recalling that $c^* = 2c_w/hh_w$, with $h = 3$ mm and $h_w = 100$ mm, leads to a critical diffusivity of 2×10^{-9} m^2 s^{-1}. This is several order of magnitudes less than previously estimated for the fault core, suggesting that faults of this type are sufficiently well drained to suppress shear heating from nucleating unstable slip. Note that this calculation is conservative in that we ask what value of diffusivity suppresses instability at all stiffness (read wavelengths). Earthquakes of course nucleate on finite sized patches with significant stiffness. Furthermore, we have neglected heat transfer, in this section; loss of heat will reduce the temperature, and thus pore pressure making the system yet more stable.

[41] Figure 4 shows the critical stiffness as a function of characteristic hydraulic diffusion time for adiabatic perturbations and stable friction. Note that in all cases the critical stiffness goes to zero when the condition (44) is met. In some cases (Figure 4b) the critical stiffness is nearly zero for hydraulic diffusivities considerably less than the critical value. This reinforces the conclusion that shear heating cannot nucleate unstable slip on frictionally stable faults.

[42] Figure 4c illustrates that in some cases the critical stiffness is not a monotonically decreasing function of c^*. How does increasing diffusivity, which should act to decrease the shear induced pore pressurization, cause the system to become more unstable? We can get some insight from numerical simulations of the governing equations. Figure 5 shows the behavior under undrained conditions when the spring stiffness is set exactly to the critical value (dashed curves). The initial conditions are steady state except that the initial velocity is slightly greater than the steady state value (2 cm yr^{-1}). Because the initial velocity exceeds the steady value, excess heat is generated causing the temperature, and hence the pore pressure, to increase. The increased velocity causes the stress to drop, which eventually reduces the rate of heat production, and hence pore pressure. According to the linear stability analysis the system is neutrally stable, and indeed the induced oscillations neither grow or decay with time.

[43] The solution with increased hydraulic diffusivity is shown with solid curves. Pore pressure diffusion diminishes the pore pressure increase in the first cycle relative to the undrained case. The slight increase in effective normal stress causes the shear stress to increase at the first minimum (relative to the undrained case) and an increased rate of heat production. As time goes on this causes an increase in the temperature and pressure oscillations and the system eventually becomes unstable. This behavior is similar to that observed by *Garagash and Rudnicki* [2003], where under some circumstances increased dilatancy causes the system to become less stable. Their behavior can be traced to slip and dilatancy laws that saturate at a critical displacement, whereas shear heating continues as long as slip occurs. The unexpected behavior in Figure 5 involves no saturation

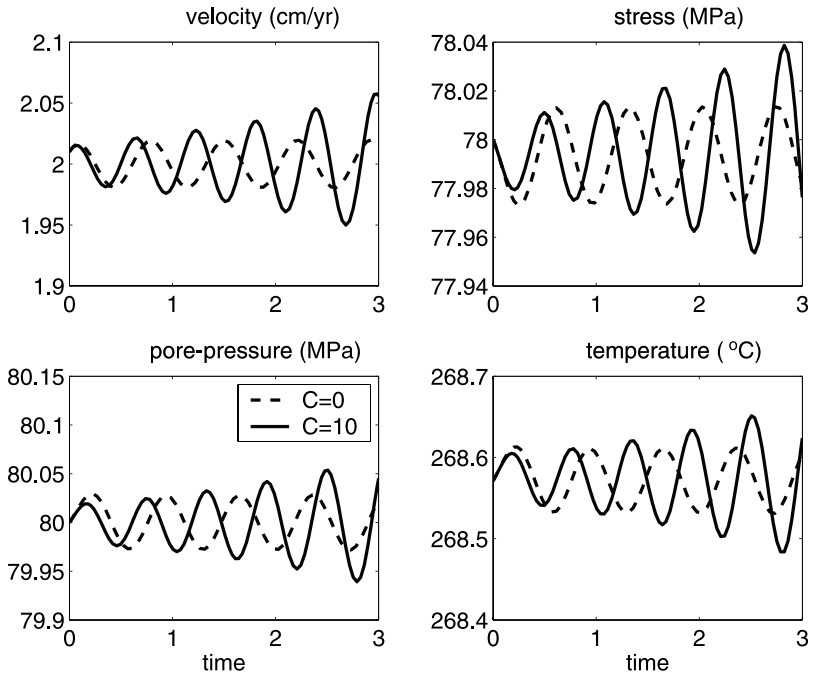

Figure 5. Increasing hydraulic diffusivity can lead to unstable behavior. The solution for $k = k_{crit}$ under undrained conditions is shown with dashed curves. The solid curves show the behavior when the diffusivity is increased to $C = 10$, and all other parameters, including spring stiffness, are held constant. The linear stability analysis predicts that the solution with increased diffusivity will be less stable.

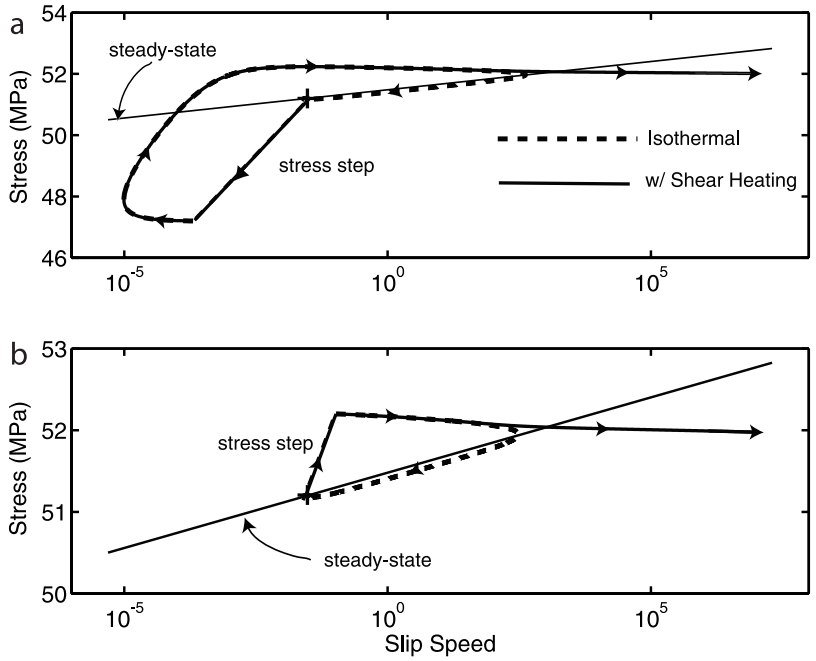

Figure 6. Shear heating can lead to unstable slip on velocity strengthening faults if the system is perturbed far from steady state. (a) Decreased stress from steady state. (b) Increased stress. In both cases the dashed curves show the paths without shear heating, in which the system evolves toward steady state (the plus sign). The solid curves show the paths with shear heating. Calculations were terminated when the velocity reached 10^7.

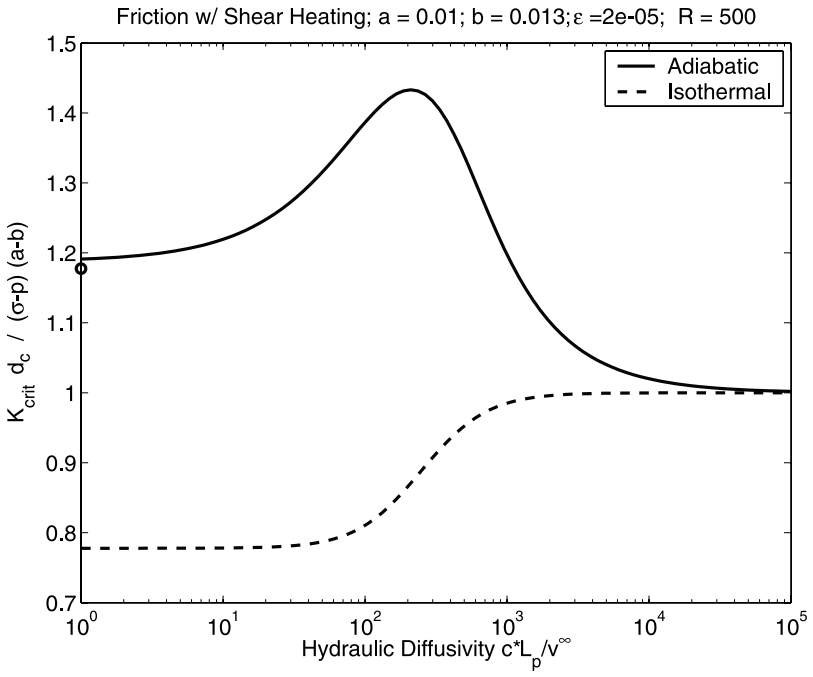

Figure 7. Normalized critical stiffness as a function of hydraulic diffusivity for adiabatic perturbations, found from roots of equation (A12). The dashed curve shows the corresponding result for isothermal conditions following *Segall and Rice* [1995]. The circle shows the prediction of the simple calculation that for undrained conditions the critical stiffness is the sum of the undrained isothermal result and the undrained adiabatic case with constant friction.

effect, resulting solely from the complex interaction between fault friction, shear heating, and pore fluid transport.

[44] To restate the conclusions of this section, (1) shear heating alone cannot nucleate unstable slip given measured permeability structure in exhumed fault zones and laboratory derived constitutive parameters, and (2) nonlinear interactions can cause unexpected behavior; in special circumstances, increased permeability causes shear heating to become more unstable.

[45] The analysis above is restricted to small perturbations from a steady state at a slip rate of order of a plate velocity. If the system is far from steady state we can expect the behavior to be qualitatively different. In particular, if the system obtains a sufficiently high velocity then shear heating effects can be expected to become important, possibly resulting in instability.

[46] *Rice and Gu* [1983] and *Ranjith and Rice* [1999] considered the behavior of a single degree of freedom system ignoring the load point motion. They showed that for velocity strengthening friction, systems raised to stresses above the steady state line initially accelerate before turning back to lower slip speeds. For sufficiently high initial stresses the maximum velocities could become sufficiently large for shear heating effects to come into play. Figure 6b shows an example of this phenomenon.

[47] Interestingly enough, decreasing the stress at constant state can have the same effect (Figure 6a) when the system is driven by a constant load point velocity. A sudden stress drop that decreases the slip rate to values much less than steady state causes the system to follow a trajectory that leads above the steady state line and ultimately to slip speeds where shear heating effects become dominant. Whether this could lead to repeated stick slip events on a frictionally stable fault is not presently clear.

8. Nucleation on Velocity Weakening Faults

[48] We now consider the behavior when the friction itself is unstable so that both frictional weakening and shear heating contribute to the accelerating fault slip. Pore pressure diffusion influences the two instabilities in opposite ways. In the isothermal case, where frictional weakening causes instability, fluid diffusion into the fault counteracts dilatancy, and is thus destabilizing. In the case of the shear heating instability with stable friction, fluid pore pressure diffusion out of the fault zone limits thermally induced pressurization, and is thus stabilizing, although as we have seen in section 7 exceptions occur.

[49] For simplicity, we first consider the case with no fluid transport and no dilatancy. The stability analysis is given in Appendix A. For typical values of $a \sim 0.01$ and $\mu_0 \sim 0.6$, $a/\mu_0 \ll 1$. We previously estimated L_p to be in the range of 12 to 18 mm, which is 2–3 orders of magnitude greater than laboratory estimates of d_c. For $a/\mu_0 \ll 1$ and $L_p/d_c \gg 1$ we show in Appendix A that the critical stiffness is given by

$$k_{uaw} = (\sigma - p)\left[\frac{(b-a)}{d_c} + \frac{\mu_0}{L_p}\right], \tag{45}$$

where the subscript uaw indicates undrained adiabatic weakening. This result is satisfying because it indicates that (in the appropriate limits) the critical stiffness is simply the sum of the isothermal frictional weakening contribution

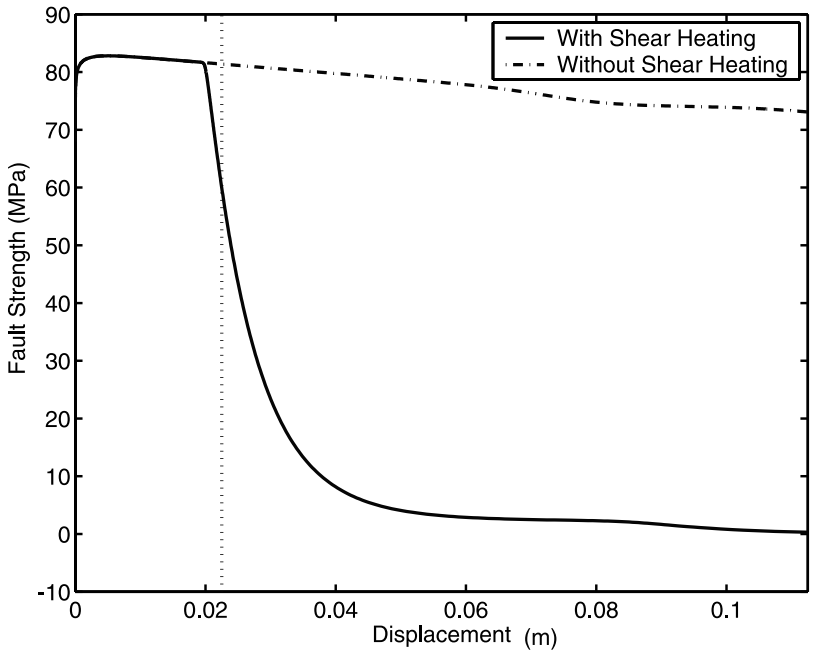

Figure 8. Fault strength (MPa) as a function of displacement (m), for two cases, one including the effect of shear heating, the other isothermal. The vertical line marks the critical displacement at which shear heating effects are expected to become significant according to equation (51). In this calculation, $a = 0.01$, $b = 0.015$, $d_c = 100\ \mu m$, $\sigma - p^{\infty} = 130$ MPa, $v^{\infty} = 0.02$ m yr^{-1}, $H = 121$, and $v^{\infty}/c^*L_p = 6 \times 10^{-7}$.

and the adiabatic shear heating contribution for constant friction.

[50] The critical stiffness for more general, adiabatic perturbations, including both pore pressure diffusion and dilatancy, is found from the roots of equation (A12) in Appendix A and illustrated in Figure 7. When the normalized diffusivity is very large the critical stiffness approaches the drained limit, k_{di}. In contrast, for undrained conditions the stiffness is the sum of the shear heating and frictional weakening contributions as predicted by (45). Figure 7 shows that there is an intermediate value of diffusivity which is least stable. The diffusivity is sufficiently high to negate dilatancy strengthening but not so high as to dissipate the pore pressures resulting from shear heating. It should be emphasized that based on field measurements of permeability structure in exhumed faults that nucleation is insensitive to shear heating effects. To see this, note that $c^*L_p/v^{\infty} = 2\ c_w L_p/hh_w v^{\infty} \sim 10^6$. This is sufficiently large for the fault to remain drained at this time scale (Figure 7).

9. When Do Shear Heating Effects Become Significant?

[51] While shear heating effects are not significant near neutral stability, they will become increasingly important as the slip speed increases. The effects of shear heating become significant when the rate of thermal pressurization exceeds the rate of pore pressure diffusion. For adiabatic deformation of a thin shear zone the rate of pressurization due to shear heating is $(\sigma - p)\ v/L_p$, so that a characteristic time for the effective stress to drop to zero is L_p/v. The ratio of thermal pressurization time to diffusion time is thus $L_p c^*/v$, and we expect that thermal effects will become significant when this ratio is order unity.

[52] For the simple model with a low-permeability fault core surrounded by effectively infinitely permeable rocks the characteristic pore pressure diffusion time is given by (23). Thus the rate of pore pressure build up exceeds the diffusion rate for

$$v > \frac{2L_p c_{\mathrm{wall}}}{hh_w}. \tag{46}$$

Taking values discussed previously leads to critical slip speeds of order 1 mm s^{-1}. When slip rates exceed this value the fault becomes undrained (we have already assumed it to be adiabatic) and the shear strength begins to drop exponentially (as in Figure 2).

[53] We can use the solution for evolution of the slip speed under drained conditions to determine the characteristic displacement at which shear heating effects become dominant. Following the procedure of *Dieterich* [1992], when the initial velocity exceeds the characteristic time for state evolution, the slip speed accelerates according to

$$v = \left(\frac{1}{v_0} - \frac{Ht}{a}\right)^{-1}, \tag{47}$$

where v_0 is the initial speed and

$$H = \left(\frac{b}{d_c} - \frac{k}{\sigma - p}\right). \tag{48}$$

Combining the condition $L_p c^*/v = 1$ with (47) yields

$$\frac{1}{v_0} - \frac{Ht}{a} = \frac{1}{L_p c^*} = \frac{t_f}{L_p}. \tag{49}$$

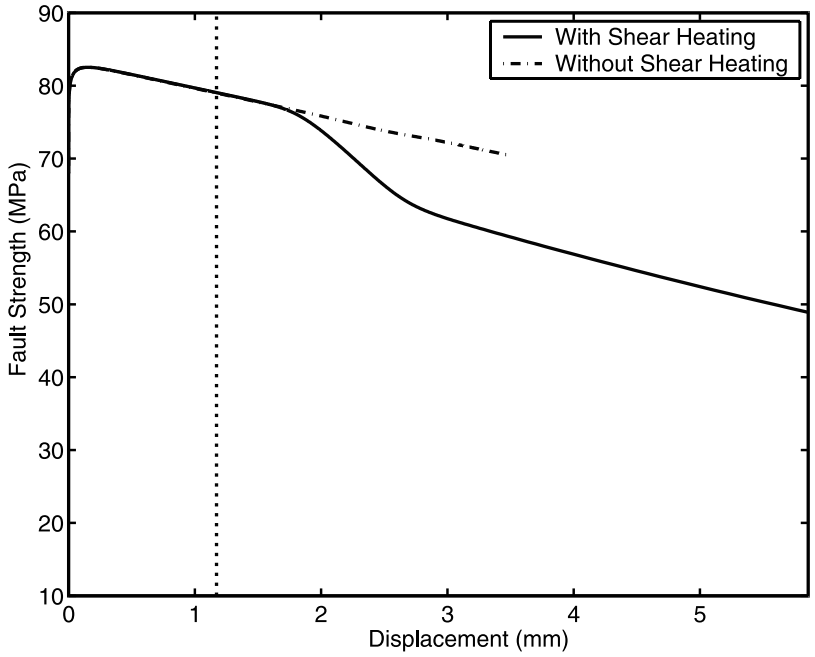

Figure 9. Fault strength (MPa) as a function of displacement (m), for two cases, one including the effect of shear heating, the other isothermal. The vertical line marks the critical displacement at which shear heating effects are expected to become significant according to equation (51). In this calculation, $a = 0.01$, $b = 0.015$, $d_c = 3$ mm, $\sigma - p^\infty = 130$ MPa, $v^\infty = 0.02$ m yr^{-1}, $H = 4.3$, and $v^\infty/c^* L_p = 6 \times 10^{-5}$.

Integrating (47) gives the displacement history for the drained system

$$u = -\frac{a}{H} \ln\left(1 - \frac{H v_0 t}{a}\right). \tag{50}$$

Combining (49) and (50) then yields the critical displacement at which shear heating effects become important

$$u_{\text{crit}} = -\frac{a}{H} \ln\left(\frac{t_f v^\infty}{L_p}\right), \tag{51}$$

where we have taken the initial velocity to be v^∞, that is the velocity at peak stress. This result is approximate in that we have neglected the effect of thermal pressurization on the slip speed in equation (47). From (48) the minimum value of H, and thus maximum value of u_{crit} occurs for the maximum elastic stiffness k, which we can take to be k_{di}, equation (42). Thus the minimum value of H is a/d_c, so that $u_{\text{crit}} = d_c \ln (L_p/t_f v^\infty)$. For $L_p \sim 10$ mm and t_f of order 10^1 to 10^2 s, the critical displacement is of order 0.1 mm.

[54] Figures 8 and 9 show computed strength as a function of displacement for two different sets of parameters. Initially the fault strength follows the elastic unloading line $-ku$. This reflects the fact that at low velocities where inertial effects are insignificant, quasi-static equilibrium requires that the shear stress and fault strength are equal. At some point the slip speed becomes sufficiently fast the further slip is undrained and adiabatic. In both examples equation (51) does a reasonably good job of predicting the onset of thermal weakening.

[55] The previous result is restricted to the case of adiabatic deformation. How much does heat conduction out of the shear zone delay the onset of shear heating instability? To address this question, we consider the planar fault model. It can be shown that the temperature change on fault from shear heating is given by (26). The velocity history in the absence of shear heating is given by (47). Thus the temperature, ignoring the feedback of the pore pressure change on the effective stress, is given by

$$\begin{aligned} T(y=0,t) &= \frac{1}{\sqrt{2\pi}} \frac{\tau_0}{\rho c} \int_0^t \frac{\left[v_0^{-1} - Ht'/a\right]^{-1} dt'}{\sqrt{2c_{th}(t-t')}} \\ &= \frac{\tau_0}{\rho c} \sqrt{\frac{va}{\pi H c_{th}}} \tan^{-1}\left(\sqrt{v/v_0 - 1}\right). \end{aligned} \tag{52}$$

Note that we can safely assume that $v/v_0 \gg 1$ so that $\tan^{-1}(\sqrt{v/v_0 - 1}) \to \pi/2$.

[56] For diffusion of heat and pore fluid into uniform half-spaces bounding the fault, equation (25) relates pore pressure and temperature directly. Thus the pore pressure in the fault zone is given by

$$p(y=0,t) = \frac{\sqrt{\pi}}{2} \frac{\Lambda}{\rho c_v} \frac{\tau_0}{\sqrt{c_{th}} + \sqrt{c_{\text{hyd}}}} \sqrt{\frac{va}{H}}. \tag{53}$$

Time enters because slip speed $v(t)$ is time-dependent.

[57] While (53) ignores the feed back of pore pressure change on the rate of frictional work, it should be approximately accurate early in the nucleation phase. To assess the importance of the shear heating relative to the frictional weakening, we consider

$$\dot{\tau} = \dot{\mu}(\sigma - p) - \mu \dot{p}. \tag{54}$$

Early in the nucleation phase when inertial effects are safely ignored, the loss of frictional strength must be balanced by a loss in driving stress $\dot{\mu}\,(\sigma - p) = -kv$. Thus a measure of the relative importance of shear heating is given by the ratio $\mu\,\dot{p}/kv$. This ratio can be used to estimate critical slip speeds at which shear heating effects become significant. We should verify that as expected from the adiabatic analysis, that these speeds are comfortably in the quasi-static regime so that inertial terms can be neglected. Dimensional analysis indicates that inertial effects become important when the slip speed exceeds $a(\sigma - p)/\eta = 2a(\sigma - p)\ v_s/G$ where η is the radiation damping coefficient, or speeds of order 0.1 m s^{-1}.

[58] The ratio $\mu\,\dot{p}/kv$ is minimum when k is maximum. The stiffness k cannot exceed the critical stiffness for unstable slip to nucleate. Simulations by *Dieterich* [1992] and *Rubin and Ampuero* [2005] indicate that nucleation (at least for modest a/b) occurs on zones with stiffness in the vicinity of k_{crit}. We thus conservatively set k to $k_{di} = (\sigma - p)(b - a)/d_c$. The rate of pore pressure change is then given by

$$\frac{\partial p(y=0,t)}{\partial t} = \frac{\sqrt{\pi}}{4}\frac{\Lambda}{\rho c_v}\frac{\mu_0(\sigma - p)}{\sqrt{c_{th}} + \sqrt{c_{\mathrm{hyd}}}}\sqrt{\frac{Hv^3}{a}}, \tag{55}$$

where we have made use of the fact that for the prescribed velocity path (equation (47)) $\dot{v} = Hv^2/a$. Thus the ratio $\mu\,\dot{p}/kv$ is

$$\frac{\mu}{kv}\frac{\partial p}{\partial t} = \frac{\sqrt{\pi}}{4}\frac{\Lambda}{\rho c_v}\frac{\mu_0^2 d_c}{(b-a)}\frac{1}{\sqrt{c_{th}} + \sqrt{c_{\mathrm{hyd}}}}\sqrt{\frac{Hv}{a}}. \tag{56}$$

This leads to a critical velocity beyond which the fault is weakening faster due to thermal pressurization than by frictional processes,

$$v_{\mathrm{crit}} = \frac{a}{\pi H}\left[\frac{4(b-a)\rho c_v\left(\sqrt{c_{th}} + \sqrt{c_{\mathrm{hyd}}}\right)}{\mu_0^2 d_c \Lambda}\right]^2. \tag{57}$$

In order to bound v_{crit}, we consider the smallest possible value of H, which following earlier arguments we take to be a/d_c, so that v_{crit} should not exceed

$$v_{\mathrm{crit}} = \frac{1}{\pi d_c}\left[\frac{4(b-a)\rho c_v\left(\sqrt{c_{th}} + \sqrt{c_{\mathrm{hyd}}}\right)}{\mu_0^2 \Lambda}\right]^2. \tag{58}$$

Notice that increasing either the hydraulic or thermal diffusivity diminishes the rate of thermal weakening and increases v_{crit}. Increasing $(b - a)/d_c$ makes the fault more frictionally unstable, thereby increasing v_{crit}. On the other hand, increasing the thermal pressurization factor Λ decreases v_{crit}.

[59] The greatest uncertainty in the parameters is in the frictional weakening distance d_c and the hydraulic diffusivity, c_{hyd}. Taking reasonable estimates; $d_c \sim 50\ \mu$m and $c_{\mathrm{hyd}} \sim 3 \times 10^{-6}$ m^2 s^{-1}, along with $b - a = 4 \times 10^{-3}$ yields an estimate of v_{crit} of 0.7 mm s^{-1}. Increasing the hydraulic diffusivity by a factor of 3 to 10^{-5} m^2 s^{-1} increases the critical slip speed to 2 mm/s. Further decreasing d_c to 10 μm would increase v_{crit} to 10 mm s^{-1}, which is essentially an upper bound on this parameter. A plausible range of values is from the order of 10^{-2} to 10^{1} mm s^{-1}. Note that these values are in the range where inertial effects can be neglected justifying our assumption that $\dot{\mu}\,(\sigma - p) = -kv$.

10. Discussion

[60] Our analysis indicates that shear heating effects alone are neither able to initiate slip instabilities on velocity strengthening faults, nor contribute significantly to the initial nucleation of unstable slip on faults that are frictionally velocity weakening. Scaling arguments and specific analysis for slip on an interface separating uniform half-spaces indicates, however, that shear heating-induced thermal pressurization becomes important at slip speeds of the order of 1 mm s^{-1} and displacements of order 0.1 mm. There are significant uncertainties in many of the material parameters, particularly permeability of the slip zone and its immediate surroundings as well as the critical slip weakening distance in the friction law. Dilatancy during rapid accelerating slip could increase permeability, thereby decreasing the pore pressure and delaying the onset of thermally induced weakening. Changes in permeability due to decreasing effective stress which may delay the onset of thermal weakening have not been analyzed here. Nevertheless, if permeabilities estimated from the Nojima Fault, Median Tectonic Line, and other faults are representative of conditions at seismogenic depths, then it appears that shear heating effects must become important late in the nucleation process, well before detectable seismic waves are radiated off the fault.

[61] This conclusion is markedly different from those of *Kanamori and Heaton* [2000] and *Andrews* [2002], who suggest that shear heating effects become important only for $M_w = 3$ to 4 earthquakes. A significant increase in stress drop would be predicted for events larger than this threshold, a change that is not observed. It should be noted that *Andrews* [2002] assumed a hydraulic diffusivity of order 10^{-2} m^2 s^{-1}, 3–4 orders of magnitude greater than measured on ultracataclasite fault cores subject to effective stresses representative of crustal earthquake depths. Using his formula for the rupture distance before thermal pressurization becomes important, but decreasing the hydraulic diffusivity to a more reasonable 10^{-5} m^2 s^{-1}, and keeping all other parameters fixed, gives a rupture distance of 0.3 m. While it is probably unreasonable to imagine a dynamically propagating shear rupture this short, it emphasizes that our disagreement with *Andrews* [2002] is due to choice of parameters used as opposed to fundamental theoretical differences.

[62] This result that shear heating becomes significant late in the nucleation process has important implications for both earthquake occurrence and dynamic rupture. For earthquake nucleation following (47) the time to instability is given by a/Hv_0. As before, we can take $H \sim a/d_c$ for critical nucleation patches so that the time to instability is essentially d_c/v_0. Thus, from the time that shear heating effects become important to inertial instability is of order 10^{-1} s. This demonstrates that *Dieterich*'s [1994] analysis of seismicity rate variations based on rate state friction alone should not be biased by thermal effects.

[63] However, once slip rates exceed order of 1 mm s^{-1} shear heating effects may dominate changes in strength due to changes in rate and state friction (at least as understood at slow slip speeds), although the paucity of laboratory experiments at high slip speed make strong conclusions difficult. Indeed, *Rice* [2006] has shown that shear fracture energies computed assuming slip on a planar interface, with constant coefficient of friction reduced by flash heating at asperity contacts, and spatially uniform thermal and hydraulic properties are in plausible agreement with seismologically determined estimates, when allowance is made for increases of permeability and drained compressibility relative to values for intact gouge, due to off-fault damage in the concentrated stress field at the rupture front. This is true not only for the average fracture energy, but also for its dependence on slip in different sized earthquakes. The seismological based estimates of fracture energy are not without uncertainties; however, it should be emphasized that these estimates are completely independent of the theoretical predictions. That is there are no freely adjustable parameters in the theory. This agreement is strong motivation for considering the importance of thermal weakening processes during rapid slip in earthquakes.

11. Conclusion

[64] Our results suggest that the seismic weakening process may well be divided into two distinct regimes: an early nucleation regime dominated by rate and state frictional weakening, followed by a transition to thermal pressurization late in the nucleation process. The transition to shear heating-induced thermal pressurization occurs at slip speeds of order 1 mm s^{-1} and slips of order 0.1 mm. Thermal effects including shear induced thermal pressurization and flash heating may dominate during the fast (order 1 m s^{-1}) slip in the earthquake.

Appendix A

[65] In this appendix we present a linearized stability analysis of the single degree of freedom system. The procedure follows *Segall and Rice* [1995] by linearizing the governing equations about the steady state values. In this case the governing equations are (6), (7), (9), (22), (39), and (40). We then seek solutions of the form $\Delta v = Ve^{st}$, $\Delta p = Pe^{st}$, $\Delta\theta = \Theta e^{st}$, and so on. This leads to

$$(\sigma - p)as = (\sigma - p)\frac{brs}{r+s} - \frac{\mu_0\varepsilon}{\beta}\frac{rs^2}{(c^* + s)(r+s)} - krd_c + \frac{q}{(s+c^*)}[\mu_0(\sigma - p)s - krd_c], \tag{A1}$$

where $r = v^\infty/d_c$ and $q = v^\infty/L_p$ are the inverse characteristic times for state evolution and weakening due to shear heating, respectively. Note that (A1) is cubic in s; the roots s_j, $j = 1 \ldots 3$ determine the behavior of the system. If the real parts of the roots s_j are negative for all j, the system is linearly stable. If $\Re(s_j) > 0$ for some j, then the system is unstable. Finding the roots in the general case is messy, and not very revealing. To begin, we examine some limiting cases that provide more insight.

[66] For constant friction, $a = b = 0$, undrained, $c^* = 0$, and adiabatic conditions with no dilatancy, (A1) reduces to

$$s[krd_c - q\mu_0(\sigma - p)] + qkrd_c = 0. \tag{A2}$$

Note that q, r, k, and d_c are nonnegative quantities. Thus the sign of s is determined by the sign of the quantity in brackets. From this we conclude that slip is unstable, $s > 0$, when the stiffness is less than a critical value given by $k = \mu_0(\sigma - p)/L_p$, repeated as equation (41).

[67] To consider more general cases, introduce the following dimensionless parameters:

$$\begin{aligned} A &= \frac{(\sigma - p)a}{\tau_0}, \\ B &= \frac{(\sigma - p)b}{\tau_0}, \\ S &= s/q = sL_p/v_0, \\ C &= c^*L_p/v_0, \\ R &= r/q = L_p/d_c, \\ K &= \frac{kL_p}{\tau_0}, \\ E &= \frac{\mu_0\epsilon L_p}{\beta\tau_0 d_c}. \end{aligned} \tag{A3}$$

In terms of these variables, equation (A1) becomes

$$AS = B\frac{RS}{R+S} - K - \frac{ES^2}{(C+S)(R+S)} + \frac{(S-K)}{(S+C)}. \tag{A4}$$

In the limit of constant friction $A = B = 0$ and no fluid transport $C = 0$, (A4) reduces to

$$(1 - K - E)S^2 + (R - KR - K)S - KR = 0. \tag{A5}$$

The roots of (A5), S_j, $j = 1, 2$, determine the critical stiffness. First, note that in the limit that $K \to \infty$ the roots are -1 and $-R$. Since R is nonnegative, the roots in this limit are both real and negative so that perturbations from steady state are exponentially damped. Second, note that there is no solution for $S = 0$, so that the routes must cross into the real half plane through the imaginary axis. Letting $S = \pm i\omega$, and substituting into (A5), yields

$$\begin{aligned} (K - 1 + E)\omega^2 - KR &= 0 \\ i\omega[K(R+1) - R] &= 0, \end{aligned} \tag{A6}$$

since both real and imaginary parts must vanish. The first equation gives the oscillation frequency ω at neutral stability. The second equation gives the critical stiffness $K = R/(R+1)$, which in dimensional form is $\tau_0/(L_p + d_c)$.

[68] We next consider the velocity strengthening case, with no state evolution effect and no dilatancy, $B = E = 0$. In this case, equation (A4) reduces to

$$AS^2 + (AC + K - 1)S + K(C - 1) = 0. \tag{A7}$$

The roots of (A7), S_j, $j = 1, 2$, determine the critical stiffness. First, note that in the limit that $K \to \infty$ the roots

are $-K/A$ and $-(C-1)$. The parameters K, A, C are all nonnegative. Reasonable estimates of C based on our previous estimates of the characteristic diffusion time, imply that $C \gg 1$. For example, for $c^* \sim 10^{-1}$ m s^{-1}, $L_p \sim 10$ mm, and $v_0 \sim 30$ mm yr$^{-1} \approx 10^{-9}$ m s^{-1}, $C \sim 10^5$. Thus, in the limit that K becomes infinite, the real part of S is negative, so that all perturbations from steady state are strongly damped. The critical stiffness is determined by the largest value of K for which $\Re(S_j) > 0$ for some j. Since no root $S = 0$ exists with nonzero K, (as long as $C \gg 1$) a pair of roots must cross into the positive real half plane at some point we label $S = \pm i\omega$. Substituting into (A7) and requiring that real and imaginary parts both vanish leads to

$$\begin{aligned} 0 &= -A\omega^2 + K(C-1) \\ 0 &= (AC + K - 1)\omega. \end{aligned} \tag{A8}$$

The first equation in (A8) gives ω the frequency of oscillations at neutral stability. The second yields the (nondimensional) critical stiffness, for strengthening adiabatic conditions.

$$K_{sa} = 1 - AC. \tag{A9}$$

In dimensional form this becomes equation (43).

[69] We can generalize the above result by allowing for state evolution and dilatancy. Equation (A4) is equivalent to the following cubic equation:

$$\begin{aligned} &AS^3 + [A(C+R) - BR + K - 1 + E]S^2 \\ &\quad + [(A-B)RC + K(C+R+1) - R]S \\ &\quad + KR(C+1) = 0. \end{aligned} \tag{A10}$$

We establish the roots of (A10) in the limit that K becomes infinite as follows. If S is of order K^1, then only the first two terms contribute yielding a root at $S = -K/A$. If S is of order K^0 then the first term does not contribute and in the limit $K \to \infty$ (A10) reduces to a quadratic with roots $-R/2$ and $-(C+1)$. Thus, in the limit of infinite stiffness all roots are negative and the perturbations from steady state are damped in finite time. Since no root $S = 0$ exists with nonzero K and $C \geq 0$, we assume that the first root to cross to the real half plane does so at $S = i\omega$. Substituting $S = i\omega$ into (A10) and requiring that real and imaginary parts both vanish, leads to two equations in ω^2

$$\begin{aligned} 0 &= -[A(C+R) - BR + K - 1 + E]\omega^2 + KR(C+1) \\ 0 &= -A\omega^2 + [(A-B)RC + K(C+R+1) - R]. \end{aligned} \tag{A11}$$

Eliminating ω^2 yields an expression for the critical spring stiffness K_c, that is quadratic in K

$$\begin{aligned} &(C+R+1)K_c^2 + \{(C+R+1)[(A-B)R + AC + E - 1] \\ &\quad + R[(A-B)C - 1 - A(C+1)]\}K_c \\ &\quad + R[(A-B)C - 1][(A-B)R + AC + E - 1] = 0, \end{aligned} \tag{A12}$$

which can be solved for K_c (note that the largest root is the relevant one).

[70] It is of interest to determine the value of the diffusivity (call it C_{crit}) for which the critical stiffness becomes zero, under velocity strengthening conditions $A > B$. At this point the system is linearly stable, regardless of the elastic compliance. K_c is zero when the constant term, $[(A-B)C - 1][(A-B)R + AC + E - 1]$, is zero. Note that this is satisfied if either $[(A-B)C - 1] = 0$, or $[(A-B)R + AC + E - 1] = 0$. However, the critical stiffness is the larger of the two roots of (A12). The relevant root thus is one for which a second positive root does not exist. Note that if $[(A-B)R + AC + E - 1] = 0$, a second positive root exists, $K_c = R(A + BC + 1)/(C + R + 1)$. Thus the root of interest is $[(A-B)C - 1] = 0$, and $C_{\text{crit}} = 1/(A-B)$. In dimensional form this yields equation (44).

[71] We now consider the case where the friction is itself unstable, that is steady state velocity weakening. From equation (A12) in the limit of no transport or dilatancy $C = E = 0$ we find

$$(R+1)K^2 - [(R+1)(K_{di}+1) + R(A+1)]K + R(K_{di}+1) = 0, \tag{A13}$$

where the drained isothermal (Ruina) critical stiffness (42) is given, in terms of the nondimensional quantities as $K_{di} = (B-A)/R$.

[72] We now note that in the limit that $R \gg 1$ and $A \ll 1$, consistent with experimental data and assumed fault zone thickness, the quadratic above has the trivial solution

$$K_{uaw} = K_{di} + 1. \tag{A14}$$

which in dimensional form is (45).

Notation

a, b	friction constitutive constants.
c_{th}	thermal diffusivity, 10^{-6} m^2 s^{-1}.
c_{hyd}	hydraulic diffusivity
c_w	hydraulic diffusivity of fault core, 10^{-6} – 10^{-5} m^2 s^{-1}.
c^*	$1/t_f$.
d_c	frictional slip weakening distance.
G	elastic shear modulus.
h	thickness of central shear zone, ~1 mm.
h_w	thickness of wall zone (fault core), ~100 mm.
H	weakening parameter, equation (48).
k	spring stiffness.
k_{uacf}	critical stiffness for undrained adiabatic constant friction.
k_{di}	critical stiffness for drained isothermal.
k_{sa}	critical stiffness for strengthening adiabatic.
k_{uaw}	critical stiffness for undrained adiabatic weakening friction.
$\mathcal{K}$	thermal conductivity.
L_p	weakening distance undrained-adiabatic deformation, 10 mm.
m	fluid mass per unit volume of solid.
p	pore pressure.
q_h	heat flux.
q_f	fluid mass flux.
t	time.

t_f characteristic time for fluid diffusion through fault core, 10–100 s.
T temperature.
u fault displacement.
v fault slip speed.
v^∞ rate of plate motion, 10^{-9} m s^{-1}.
y fault perpendicular coordinate.
β_f isothermal pore fluid compressibility, 6×10^{-10} Pa^{-1}.
β_ϕ isothermal pore compressibility, 0.5×10^{-9} Pa^{-1}.
β total compressibility, $\phi(\beta_f + \beta_\phi)$, $5–8 \times 10^{-11}$ Pa^{-1}.
ε dilatancy parameter.
γ shear strain.
κ permeability, $10^{-21} - 10^{-19}$ m^2 for fault core.
λ_f isobaric pore fluid expansivity, 1×10^{-3} C^{-1}.
λ_ϕ isobaric pore expansivity, -2×10^{-4} C^{-1}
Λ thermal pressurization factor, equation (19), 0.6 –1.1 MPa °C^{-1}.
ϕ pore volume per unit total volume (~ porosity); ϕ_0 in reference state.
ϕ_{plastic} plastic component of fault zone porosity.
μ coefficient of friction, μ_0 nominal value.
ν pore fluid viscosity, 1×10^{-4} Pa s.
ρ pore fluid density, ρ_0 in reference state.
$\rho_{\text{total}} c_v$ specific heat capacity, 2.7 MPa °C^{-1}.
σ fault normal stress.
τ shear stress.
θ friction state variable.

[73] **Acknowledgments.** This research was in part supported by USGS NEHRP grants 1434-HQ-96-GR-02710 and 02HQGR0120 to Stanford, and by NSF-EAR grants 0125709 and 0510193 to Harvard. We thank the Isaac Newton Institute for Mathematical Sciences of Cambridge University and the Kavli Institute for Theoretical Physics for providing venues conducive to the completion of this work. Jim Dieterich suggested that velocity strengthening systems at low stress and slip speeds might become unstable.

References

Andrews, D. J. (2002), A fault constitutive relation accounting for thermal pressurization of pore fluid, *J. Geophys. Res.*, *107*(B12), 2363, doi:10.1029/2002JB001942.

Andrews, D. J., and Y. Ben-Zion (1997), Wrinkle-like slip pulse on a fault between different materials, *J. Geophys. Res.*, *102*, 553–572.

Brune, J. N., S. Brown, and P. Johnson (1993), Rupture mechanism and interface separation in foam rubber models of earthquakes: A possible solution to the heat flow paradox and the paradox of large overthrusts, *Tectonophysics*, *218*, 59–67.

Carslaw, H. S., and J. C. Jaeger (1959), *Conduction of Heat in Solids*, 510 pp., Clarendon, Oxford, U. K.

Chester, F. M., and J. S. Chester (1998), Ultracataclasite structure and friction processes of the Punchbowl fault, San Andreas system, California, *Tectonophysics*, *295*, 199–221.

Chester, F. M., J. P. Evans, and R. L. Biegel (1993), Internal structure and weakening mechanisms of the San Andreas fault, *J. Geophys. Res.*, *98*, 771–786.

Dieterich, J. H. (1979), Modeling of rock friction: 1. Experimental results and constitutive equations, *J. Geophys. Res.*, *84*, 2161–2168.

Dieterich, J. H. (1992), Earthquake nucleation on faults with rate- and state-dependent strength, *Tectonophysics*, *211*, 115–134.

Dieterich, J. H. (1994), A constitutive law for rate of earthquake production and its application to earthquake clustering, *J. Geophys. Res.*, *99*, 2601–2618.

Garagash, D. I., and J. W. Rudnicki (2003), Shear heating of fluid-saturated slip- weakening dilatant fault zone. 1. Limiting regimes, *J. Geophys. Res.*, *108*(B2), 2121, doi:10.1029/2001JB001653.

Kanamori, H., and T. H. Heaton (2000), Microscopic and macroscopic physics of earthquakes, in *Physics of Earthquakes*, *Geophys. Monogr. Ser.*, vol. 120, edited by J. B. Rundle, D. L. Turcotte, and W. Klein, pp. 147–163, AGU, Washington, D. C.

Kilgore, B. D., J. H. Dieterich, and M. L. Blanpied (1993), Velocity dependent friction of granite over a wide range of conditions, *Geophys. Res. Lett.*, *20*, 903–906.

Lachenbruch, A. H. (1980), Frictional heating, fluid pressure, and the resistance to fault motion, *J. Geophys. Res.*, *85*, 6097–6112.

Lapusta, N., and J. R. Rice (2004), Earthquake sequences on rate and state faults with strong dynamic weakening, *Eos Trans. AGU*, *84*(46), Fall Meet. Suppl., Abstract S51B-02.

Lee, T. C., and P. T. Delaney (1987), Frictional heating and pore pressure rise due to fault slip, *Geophys. J. R. Astron. Soc*, *88*, 569–591.

Lockner, D. A., H. Naka, H. Tanaka, H. Ito, and R. Ikeda (2000), Permeability and strength of core samples from the Nojima Fault of the 1995 Kobe earthquake, in *Proceedings of the International Workshop on the Nojima Fault Core and Borehole Data Analysis, Tsukuba Japan, 22–23 November, 1999*, edited by H. Ito et al., *U.S. Geol. Surv. Open File Rep., 00-129*, 147–152.

Marone, C. (1998), Laboratory-derived friction laws and their application to seismic faulting, *Annu. Rev. Earth Planet. Sci.*, *26*, 643–696.

Marone, C., C. B. Raleigh, and C. H. Scholz (1990), Frictional behavior and constitutive modeling of simulated fault gouge, *J. Geophys. Res.*, *95*, 7007–7025.

Mase, C. W., and L. Smith (1987), Effects of frictional heating on the thermal, hydrologic, and mechanical response of a fault, *J. Geophys. Res.*, *92*, 6249–6272.

Ranjith, K., and J. R. Rice (1999), Stability of quasi!static slip in a single degree of freedom elastic system with rate and state dependent friction, *J. Mech. Phys. Solids*, *47*, 1207–1218.

Rice, J. R. (1996), Low-stress faulting: Strong but brittle faults with local stress concentrations (abstract), *Eos Trans. AGU*, *77*(46), Fall Meet. Suppl., F471.

Rice, J. R. (1999), Flash heating at asperity contact and rate-dependent friction (abstract), *Eos Trans. AGU*, *80*(46), Fall Meet. Suppl., F681.

Rice, J. R. (2006), Heating and weakening of faults during earthquake slip, *J. Geophys. Res.*, *111*, B05311, doi:10.1029/2005JB004006.

Rice, J. R., and J. C. Gu (1983), Earthquake aftereffects and triggered seismic phenomena, *Pure Appl. Geophys.*, *121*, 187–219.

Rice, J. R., and A. Ruina (1983), Stability of steady frictional sliding, *J. Appl. Mech.*, *50*, 343–349.

Rubin, A. M., and J.-P. Ampuero (2005), Earthquake nucleation on (aging) rate and state faults, *J. Geophys. Res.*, *110*, B11312, doi:10.1029/2005JB003686.

Rudnicki, J. W., and D. A. Koutsibelas (1991), Steady propagation of plane strain shear cracks on an impermeable plane in an elastic diffusive solid, *Int. J. Solids Struct.*, *27*, 205–225.

Rudnicki, J. W., and J. R. Rice (2006), Effective normal stress alteration due to pore pressure changes induced by dynamic slip propagation on a plane between dissimilar materials, *J. Geophys. Res.*, doi:10.1029/2006JB004396, in press.

Ruina, A. (1983), Slip instability and state variable friction laws, *J. Geophys. Res.*, *88*, 10,359–10,370.

Segall, P., and J. R. Rice (1995), Dilatancy, compaction, and slip instability of a fluid saturated fault, *J. Geophys. Res.*, *100*, 22,155–22,171.

Sibson, R. H. (1973), Interactions between temperature and pore-fluid pressure during earthquake faulting and a mechanism for partial or total stress relief, *Nature*, *243*(126), 66–68.

Sibson, R. H. (2003), Thickness of the seismic slip zone, *Bull. Seismol. Soc. Am.*, *93*(3), 1169–1178, doi:10.1785/0120020061.

Sleep, N. H. (1995), Frictional heating and the stability of rate and state dependent frictional sliding, *Geophys. Res. Lett.*, *22*, 2785–2788.

Sleep, N. H., and K. Fujita (1997), *Principles of Geophysics*, Blackwell Sci., Malden, Mass.

Townend, J., and Mark D. Zoback (2000), How faulting keeps the crust strong, *Geology*, *28*(5), 399–402, doi:10.1130/0091-7613(2000).

Tullis, T. E., and D. L. Goldsby (2003), Flash melting of crustal rocks at almost seismic slip rates, *Eos Trans. AGU*, *84*(46), Fall Meet. Suppl., Abstract S51B-05.

Weertman, J. (1980), Unstable slippage across a fault that separates elastic media of different elastic constants, *J. Geophys. Res.*, *85*, 1455–1461.

Wibberley, A. J. (2002), Hydraulic diffusivity of fault gouges and implications for thermal pressurization during seismic slip, *Earth Planets Space*, *54*, 1152–1171.

Wibberley, A. J., and T. Shimamoto (2003), Internal structure and permeability of major strike-slip fault zones: The Median Tectonic Line in Mie prefecture, southwest Japan, *J. Struct. Geol.*, *25*, 59–78.

J. R. Rice, Department of Earth and Planetary Sciences, Harvard University, Cambridge, MA 02138, USA. (rice@esag.harvard.edu)

P. Segall, Department of Geophysics, Stanford University, Stanford, CA 94305, USA. (segall@pangea.stanford.edu)